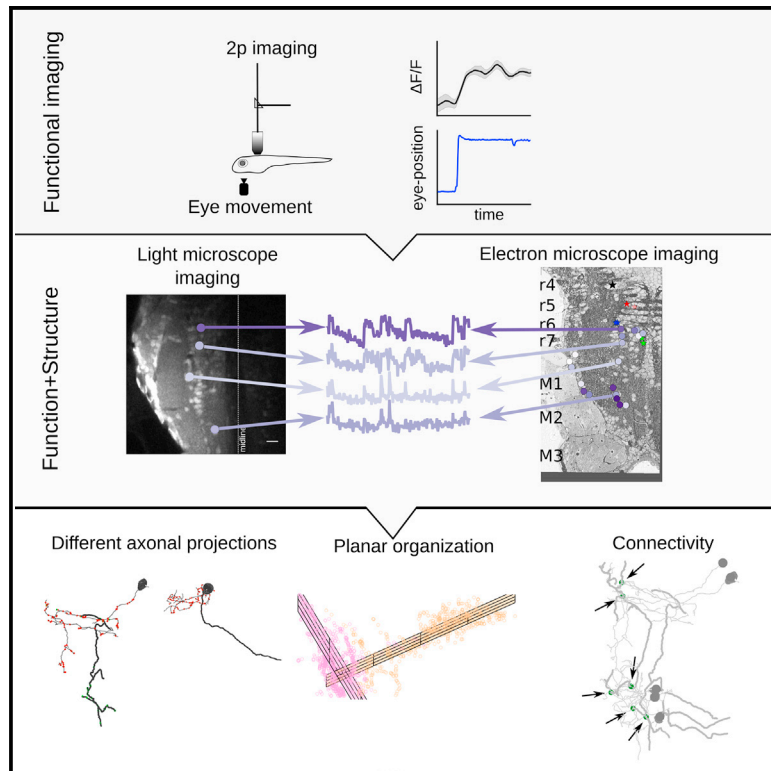


Electron Microscopic Reconstruction of Functionally Identified Cells in a Neural Integrator

Graphical Abstract



Authors

Ashwin Vishwanathan, Kayvon Daie, Alexandro D. Ramirez, Jeff W. Lichtman, Emre R.F. Aksay, H. Sebastian Seung

Correspondence

ashwinv@princeton.edu (A.V.), sseung@princeton.edu (H.S.S.)

In Brief

Vishwanathan et al. combined two-photon calcium imaging and serial-section electron microscopy in the larval zebrafish to reconstruct neurons in the oculomotor integrator. They observed three classes of neurons and evidence of synaptic connections between these classes.

Highlights

- Correlated light and electron microscopy from larval zebrafish
- Electron microscopic reconstruction of neurons encoding for eye-movement behavior
- Imaged neurons differed in axonal projections, dendritic arbors, and synaptic densities
- Synaptic connections between integrator cells



Electron Microscopic Reconstruction of Functionally Identified Cells in a Neural Integrator

Ashwin Vishwanathan,^{1,5,*} Kayvon Daie,³ Alexandro D. Ramirez,³ Jeff W. Lichtman,⁴ Emre R.F. Aksay,³ and H. Sebastian Seung^{1,2,*}

¹Neuroscience Institute

²Computer Science Department

Princeton University, Princeton, NJ 08544, USA

³Institute for Computational Biomedicine and Department of Physiology and Biophysics, Weill Cornell Medical College, New York, NY 10021, USA

⁴Department of Molecular and Cellular Biology and Center for Brain Science, Harvard University, Cambridge, MA 02138, USA

⁵Lead Contact

*Correspondence: ashwinv@princeton.edu (A.V.), sseung@princeton.edu (H.S.S.)

<http://dx.doi.org/10.1016/j.cub.2017.06.028>

SUMMARY

Neural integrators are involved in a variety of sensorimotor and cognitive behaviors. The oculomotor system contains a simple example, a hindbrain neural circuit that takes velocity signals as inputs and temporally integrates them to control eye position. Here we investigated the structural underpinnings of temporal integration in the larval zebrafish by first identifying integrator neurons using two-photon calcium imaging and then reconstructing the same neurons through serial electron microscopic analysis. Integrator neurons were identified as those neurons with activities highly correlated with eye position during spontaneous eye movements. Three morphological classes of neurons were observed: ipsilaterally projecting neurons located medially, contralaterally projecting neurons located more laterally, and a population at the extreme lateral edge of the hindbrain for which we were not able to identify axons. Based on their somatic locations, we inferred that neurons with only ipsilaterally projecting axons are glutamatergic, whereas neurons with only contralaterally projecting axons are largely GABAergic. Dendritic and synaptic organization of the ipsilaterally projecting neurons suggests a broad sampling from inputs on the ipsilateral side. We also observed the first conclusive evidence of synapses between integrator neurons, which have long been hypothesized by recurrent network models of integration via positive feedback.

INTRODUCTION

Combining two-photon calcium imaging with serial electron microscopy (EM) is an emerging approach for studying the structure and function of neural circuits at cellular resolution. In the mouse retina [1] and primary visual cortex [2, 3], this approach

has been used to study the structure and function of visual neurons. Here we apply this approach to a population of neurons defined by their encoding of behavioral variables, rather than stimulus variables. Namely, we focus on neurons that carry horizontal eye-position signals that are located in a hindbrain neural circuit known as the “horizontal velocity-to-position neural integrator,” or “neural integrator” for short [4, 5]. Our study is done in the larval zebrafish, which has emerged as an important model organism for investigating the relation between neural circuits and behavior [6].

The neural integrator gets its name because the transformation of eye velocity into eye position is the computational operation of integration with respect to time. Integrator neurons carry a horizontal eye-position signal in their spiking during fixations, and lesion or inactivation of these cells leads to pronounced deficits in the ability to maintain gaze fixation [7–9]. Integrator neurons are thought to send their eye-position signals to extraocular motor neurons through monosynaptic and polysynaptic pathways [10–12]. They are also thought to receive inputs from multiple convergent pathways that encode eye velocity for every type of eye movement [13, 14]. Therefore, the neural integrator is the “final common pathway” for all types of eye movements in fish [15–17], rodents [18], non-human primates [19, 20], and humans [21].

Most investigations of the structural underpinnings of neural integration in the oculomotor system have relied on combining single-neuron electrophysiology with light microscopic dye fills. Intracellular recordings in goldfish hindbrain neurons that exhibited spiking correlated to eye position, followed by anatomical dye fills, show that the axons of these neurons send collaterals to areas where other integrator neurons were observed [16]. Similar anatomical observations have been observed in cats [22] and non-human primates [23]. These observations have shaped theoretical models proposing that integration can be supported by positive feedback between these neurons [24–28]. More recently, calcium imaging approaches using two-photon microscopy to identify many integrator neurons have been coupled with sparse, targeted single-neuron electroporation of fluorescent indicators for anatomical reconstruction [29]. All of these studies have delineated the arborization and projection patterns of integrator neurons, but were limited to

one or a few neurons in any individual brain and do not reveal locations and distributions of their input and output synapses. Furthermore, although the axonal projections could indicate the presence of synapses onto dendrites of other integrator neurons, conclusive evidence has been lacking.

We combined two-photon calcium imaging and serial EM to determine both the function and structure of neurons throughout the oculomotor neural integrator. We found evidence for multiple classes of neurons within the integrator population based on differences in dendritic arborization, axonal projections, and synaptic distributions. These included neurons at medial locations with ipsilaterally projecting axons that were inferred to be excitatory, and neurons at more lateral locations with contralaterally projecting axons that were inferred to be inhibitory. Furthermore, we identified the locations of all chemical synapses onto and from the imaged integrator population, and inferred from ultrastructural properties of vesicles that these synapses were of the conventional rather than peptidergic variety. Finally, we report evidence for direct synaptic connectivity between integrator neurons.

RESULTS

Combined Two-Photon and EM of Integrator Neurons

To identify integrator neurons, we performed two-photon light microscopy (LM) imaging of the caudal hindbrain in a larval zebrafish at 6 days post-fertilization following bolus loading of the calcium sensor Oregon green BAPTA 1-AM. The functional imaging was restricted to one side where the loading was best and performed on three planes that were $\sim 8 \mu\text{m}$ apart during spontaneous eye movement. Calcium signals were correlated with eye position to identify integrator somata from the imaged planes (Figure 1A) [30]. Neurons were identified as integrator neurons if saccade-triggered eye position following an ipsiversive saccade (Figure 1Ab, arrows) was correlated with saccade-triggered average fluorescence (Figure 1Ac, first column) (Pearson coefficient $r > 0.6$). The integration time constants or the level of persistence was quantified as the time constant of an exponential fit to the firing rate profile determined from a deconvolution of the fluorescence data (Figure 1Ac, dotted lines; STAR Methods). This resulted in the identification of 22 integrator neurons with graded levels of persistence (Figures S1A–S1C).

Following functional identification of integrator neurons, the tissue was fixed, stained, sectioned for serial EM and imaged at a final resolution of $5 \times 5 \times 45 \text{ nm}$ (RC, rostral-caudal; ML, medio-lateral; DV, dorso-ventral). These images were montaged and aligned to create a 3D EM volume (Figure 1B; STAR Methods). The resulting EM volume extended ventrally from the Mauthner cell axon plane by $\sim 60 \mu\text{m}$, caudally from the border of rhombomeres 5/6 by $\sim 200 \mu\text{m}$, and laterally from the midline by $\sim 100 \mu\text{m}$. The LM and EM volumes were registered to each other by an affine transform, producing correspondence of labeled neurons and blood vessels (Figure 1C; Figure S1D; STAR Methods). The somata of all 22 integrator neurons from the LM volume were located in the EM volume and distributed throughout the caudal hindbrain and along the border between rhombomeres 6 and 7 (Figure 1D, colored by time constants).

Stripe-like Patterning of Somata in the Hindbrain

Cell bodies in the hindbrain of the larval zebrafish follow a stereotypical stripe-like pattern of alternating cell bodies and neuropil. Cells within the same stripe typically share the same neurotransmitter identity and morphology [31–33]. To extract this stripe-like organization, we projected the locations of all cell somata (Figure 1D, circles) from the high-resolution imaged area onto a single plane. The high-resolution EM volume contained a total of 2,967 somata spread over rhombomeres 5 through 8 (Figure 1D). The volume also contained well-known landmarks such as the Mauthner neuron [34], the axon of the contralateral Mauthner neuron, neurons MiD2 and MiD3 of the reticulo-spinal network [34], and a number of commissural bundles (Figure 1D). This procedure revealed an alternating pattern of cell somata and neuropil. We were able to locate three peaks of cell somata, excluding a peak that corresponds to neurons at the midline, each corresponding to a likely stripe (Figure 1D, bottom panel, S1–S3). The three stripes were labeled based on their proximity to the midline as medial (S1), intermediate (S2), and lateral stripe (S3). The medial-most stripe S1 aligns with a group of neurons that express the *alx* transcription factor and are predominantly glutamatergic [29, 32, 35]. The intermediate stripe S2 corresponds to neurons known to express the transcription factor *dbx1b* [32]. At the ventral locations explored here, integrator neurons in this stripe are almost exclusively GABAergic, whereas a small minority express glutamate [29] (more dorsally, this stripe is medially abutted by cells that express the *engrailed-1* transcription factor, which expresses glycine [32, 35]). The lateral-most stripe S3 corresponds to the expression of the *barhl* transcription factor, which is also thought to be glutamatergic [32, 36].

Anatomical Properties of Integrator Neurons

After the identification of the integrator neurons in the EM volume, we reconstructed all 22 integrator neurons and annotated the pre- and postsynaptic locations for these neurons (STAR Methods). We first describe some of the anatomical properties that were common to all integrator neurons.

Somata

The somatic locations of the 22 integrator neurons were distributed over $\sim 23 \mu\text{m}$ in the DV axis and along the entire RC extent of the imaged volume. The somata of integrator neurons associated with S1 were located very close to the midline and close to the rostral edge of the imaged volume, close to the border between rhombomeres 6 and 7. Somata associated with S2 were distributed along the entire RC extent of the imaged volume. Finally, somata associated with S3 were located at the lateral end of the volume in rhombomere 8. The diameters of the integrator neurons were normally distributed, with a mean of $4.5 \pm 0.6 \mu\text{m}$ (mean \pm SD). In general, the size of the somata was proportional to the persistence level of the neurons, with larger neurons exhibiting a higher degree of persistence (Figure S1B, right; $r = 0.4$, $p = 0.059$). On average, 3.3 ± 1.5 neurites emerged from the somata and traveled ventrally.

Synapses

We annotated 320 presynaptic (green circles, Figure 2) and 2,195 postsynaptic sites (red circles, Figure 2) on the 22 integrator neurons. Synapses were identified by the presence of a presynaptic vesicle pool and adjacent synaptic density.

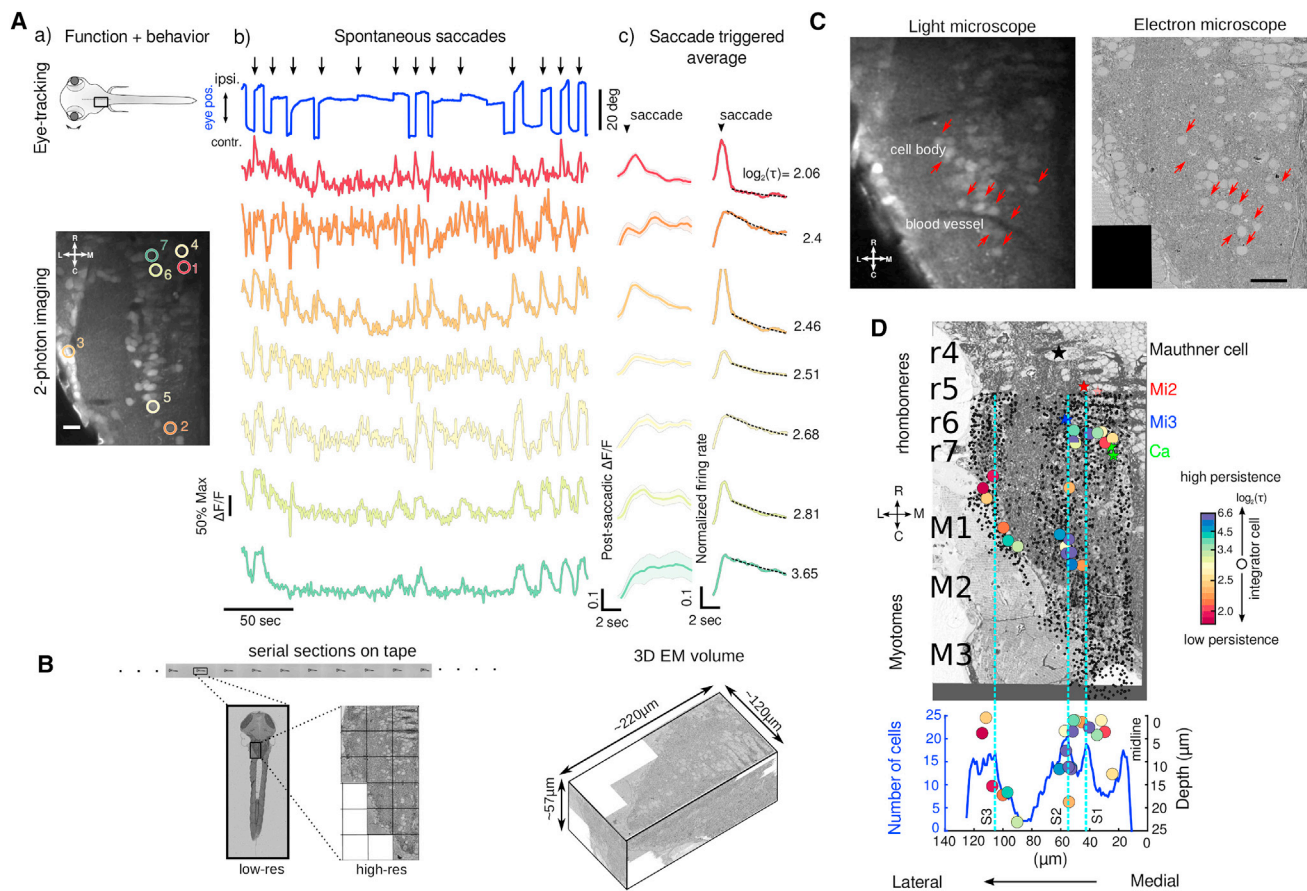


Figure 1. Functional and Structural Imaging of Integrator Neurons

(A) (a) Top: larval zebrafish schematic showing the region where functional imaging was performed (black box) located in the hindbrain. Bottom: a single imaging plane showing neurons loaded with calcium indicator Oregon green BAPTA 1-AM (OGB-1). Identified integrator neurons are shown in colored circles. Colors reflect the level of persistence of the neuron. Scale bar, 20 μm . (b) Spontaneous eye movement (top, blue line) showing saccades (sharp vertical lines) and postsaccadic fixations (horizontal lines). Ipsilateral saccades are indicated by black arrows. Colored traces below are the changes in fluorescence from individual neurons in (a). Colors represent the persistence level of the neuron. Because integrator neurons have eye-position thresholds, not all cells (green) fire throughout the eye-position range observed here. (c) Normalized fluorescence and firing rate of neurons in (a). Thick lines show the average, with shaded regions showing the SEM. Dotted lines indicate the exponential fit to determine persistence time constant, represented as $\log_2(\tau)$.

(B) Top: serial-sections for EM were collected on a tape in an automated manner. Bottom left: overview image of a single section. The region of interest that corresponds to the functionally imaged area was defined by the black box for high-resolution imaging. Bottom right: all such images were aligned to generate a 3D EM volume.

(C) Registration of LM volume to EM volume is used to locate the neurons that were involved in the behavior. Red arrows indicate the same features in both LM and EM. Scale bar, 20 μm .

(D) An example EM plane showing anatomical landmarks: Mauthner neuron (black star), Mi2 (red stars), Mi3 (blue stars), and Ca (green stars). Anatomical locations of all identified integrator neurons (colored circles) and all remaining cell bodies in the imaged EM volume (circles). Colors of the integrator neurons correspond to the persistence time of the neuron. Bottom: a distribution of all neurons along the ML axis with integrator neurons overlaid. Dotted lines (cyan) are the identified somata stripes S1–S3.

See also Figure S1.

The synaptic density was mainly confined to the cleft. It extended into the intracellular space diffusely on the presynaptic side and very little on the postsynaptic side (Figure S2E). Synapses from or onto integrator neurons contained small vesicles, presumably containing a conventional neurotransmitter. Elsewhere in the volume, we did identify synapses with dense core vesicles, presumably containing a peptide neurotransmitter (Figure S2A). The conventional distinction between symmetric and asymmetric synapses did not seem relevant. Symmetric synapses are associated with many flat vesicles, but flat vesicles were

uncommon at all synapses in our dataset. Asymmetric synapses exhibit a strong postsynaptic density, which was not observed here (Figure S2E).

Integrator Presynaptic Sites. The presynaptic site was generally at a varicosity in the axon with vesicles throughout. A small, denser cluster of vesicles was typically observed immediately adjacent to the synaptic density. These features are consistent with the idea of a presynaptic active zone. The number of presynaptic sites on a neuron averaged 57.6 ± 45.3 . This is an underestimate of the number of output synapses from an integrator

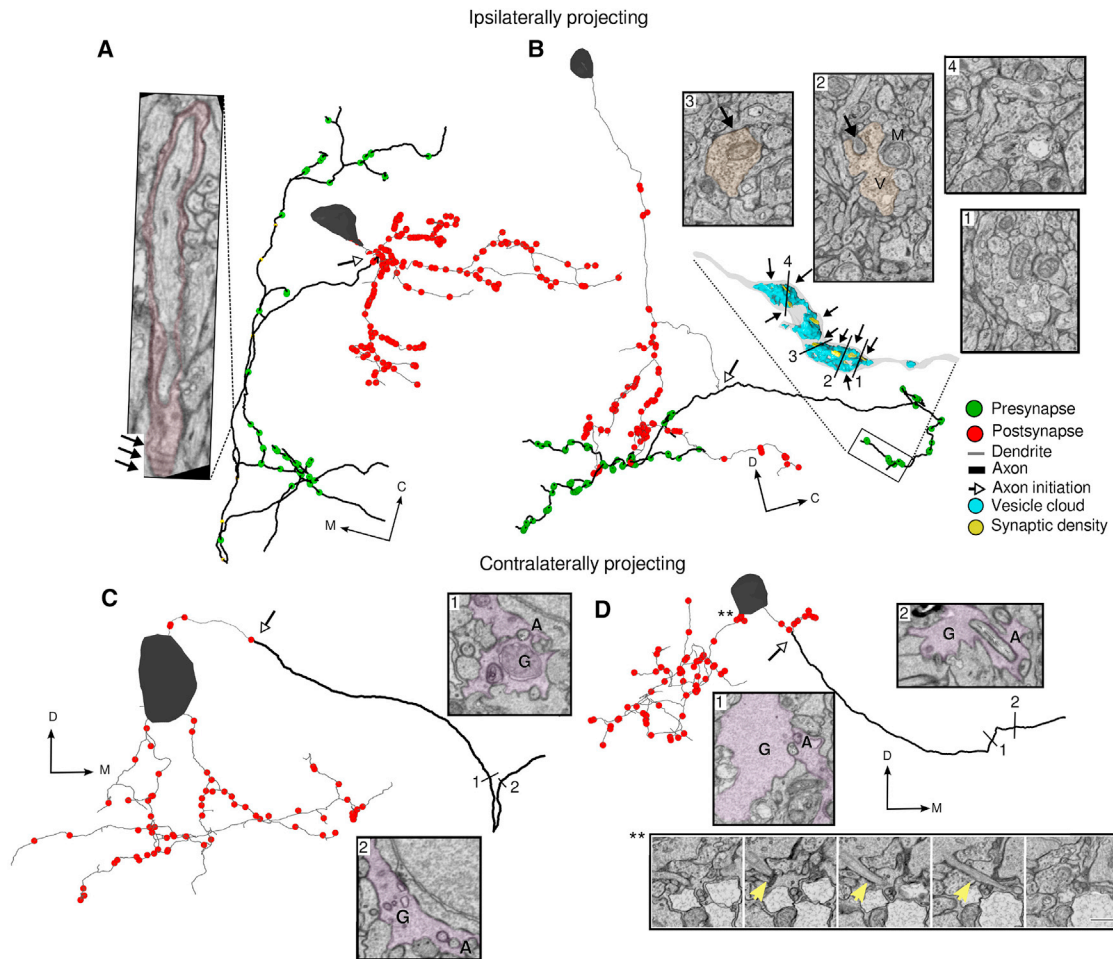


Figure 2. Ultrastructural Features of Integrator Neurons

(A) Integrator neuron with an ipsilaterally projecting axon (dark line) with presynaptic (green circles) locations and dendrites (light lines) with postsynaptic (red circles) locations. Parts of the axon of this integrator neuron are loosely myelinated (yellow circles). Right: axons with loose myelin (colored); arrows indicate individual myelin sheaths, and the open arrow shows the location of axon initiation.

(B) Integrator neuron with an ipsilaterally projecting axon. The axon is studded with presynaptic sites that are clustered along the neurite. Inset: a 3D reconstruction of the axon termination zone with a large vesicle cloud (blue) with multiple synaptic densities (yellow) opposed to the vesicles. Numbers correspond to EM insets showing the synapses. M, mitochondria; V, vesicles. Arrows show the synapses at those locations.

(C) Integrator neuron with a contralaterally projecting axon. A putative contralateral axon emerges from somata and is engulfed by glia before crossing the midline (EM insets at numbered locations; G, glia; A, axon). The open arrow indicates the axon initiation site.

(D) Integrator neurons with only a contralaterally projecting axon. A putative axon is engulfed by glia before crossing the midline (EM insets at numbered locations). Bottom EM panel: primary cilia are highlighted with yellow arrows. All of the integrator somata in this volume give rise to cilia, but it is shown for this neuron. The scale bar is 500 nm. The double asterisk represents where an anatomical structure exists, but it is not visible with this scale.

See also [Figure S2](#).

neuron, because all axonal arbors were cut off by the borders of the volume. If statistics are restricted to the three longest neurons that were more complete than others, there were 82 ± 49.3 presynaptic sites.

Integrator Postsynaptic Sites. The number of postsynaptic sites on a neuron averaged 99.7 ± 72.4 . This is a reasonable estimate of the number of input synapses to an integrator neuron, because most dendritic arbors were reconstructed in their entirety.

Cell Junctions. Along the somatic membrane, a darkening of the membrane interrupted by small gaps was often observed ([Figure S2B](#)). The darkening persisted over multiple serial sec-

tions, suggesting that it was not an artifact of tissue preparation or imaging. These darkenings were visible between somata of integrator-integrator and integrator-non-integrator neurons. We speculate that these darkenings are some kind of cell junction. Due to limited image resolution, we cannot ascertain whether these are gap junctions, which are known to exist in the developing larval zebrafish hindbrain [37].

Dendrites

Dendrites were defined by the absence of presynaptic vesicles and the presence of synaptic densities. They typically extended from somata in the ventral direction. Dendrites were smooth rather than spiny. Some dendrites exited the imaged volume,

leading to incompletely reconstructed neurons. Neurons with small dendritic arbors were completely reconstructed and did not have any dendrites that exited the imaged volume.

Axons

Neurites with presynaptic vesicles were identified as axons. Regions of transition, from dendrite to axon, we termed axon initiation sites. Example axon initiation sites are indicated in Figure 2, showing the dendrite (neurite with red postsynaptic sites) turning into axons at the axon initiation (open arrows). The main trunk of the axon extended rostrally and ventrally (Figures 2A and 2B). From the main trunk emerged branches along the ML axis, which we term collaterals (the number of collaterals we observed were similar to numbers with LM; A.V., unpublished data).

We observed sheaths around some axonal segments. In some locations, we saw that the sheath wrapped around the axon a few times, loosely enough that cytoplasmic space was visible (Figure 2A, EM panel). This fit the description of loose myelin [38], which differs from the more electron-dense compact myelin (elsewhere in the volume; data not shown). The axon of the neuron in Figure 2A was intermittently loosely myelinated along its RC section. Collaterals emerged along the ML axis from the gaps in loose myelin and remained unmyelinated. Such loose myelin sheaths have been previously reported in goldfish [39].

For 10/22 (45%) integrator neurons, neurites that cross the midline were identified as putative axons using several criteria. First, the putative axons were devoid of any postsynaptic sites on the ipsilateral side (Figures 2B and 2D, open arrow to end, no synapses). Second, before crossing the midline, the putative axon became engulfed by processes that appeared glial in nature (Figures 2C and 2D, EM insets, label G). The glial engulfment is consistent with the idea of “glial bridges” that are instrumental in the guidance of axons during development [40]. Third, these putative axons were thinner than the remaining neurites of the neuron. The diameters of these putative axons were smaller than the other neurites and similar to the diameters of conventional axons (Figure 3F). The mean axonal diameter was less than the mean dendrite diameter, conforming to the textbook notion that axons are thinner than dendrites. Putative axons could not be conclusively identified as axons, because their presynaptic sites were presumably on the contralateral side of the brain, which was not included in the imaged volume.

Small Protuberances

A small fraction (~4%, or 91/2,195) of the postsynaptic sites were located on finger-like projections from dendrites that were enveloped by invaginations of axonal boutons (Figure 2B, EM panel 2). These projections resemble structures found across multiple species called “spinules,” and are thought to be present on large, active synapses [41].

We also observed a primary cilium on all 22 integrator neurons. Primary cilia are known to be present in most, if not all, mammalian cells, including neurons, and are thought to be important for normal development [42]. The average cilium was typically ~4 μm, was enriched with microtubules, and emerged from the neuron somata very close to the Golgi complex. In some cases, this primary cilium terminated inside processes that appeared glial (Figure S2C). There was no strong orientation preference in cilium distribution (Figure S2D).

Axonal Projection Patterns of Integrator Neurons

The reconstructed integrator neurons were then divided into three groups based on the spatial projection patterns of the axons that were identified. Below we have detailed the properties of integrator neurons from each of these groups.

Ipsilateral Projection Only

Six neurons located at the rostral edge of the volume were observed to have only ipsilaterally projecting axons (Figure 3A). Two representatives are shown in Figures 2A and 2B. The axons were clearly identified by the presence of en-passant boutons with presynaptic vesicles. The somata were located at the rostral extent of the volume, close to the midline (Figure 3A, Ipsi-only). The axons were oriented along the RC axis, with the rostral end more ventral as compared to the caudal end. The average length of axons was ~260 μm (see also Table S1), with the longest reconstructed axon being 463 μm. Axons at the rostral extreme of the volume appeared to overlap with the expected location of the abducens motor nucleus (based on its known position within rhombomeres r5 and r6; Figure S3A), with terminations in r4 as well. Two of the six axons had projections that terminated near the site of the abducens motor nuclei and projected further rostrally (Figure S3B). None of the axons were observed emerging directly from the somata. Instead, dendrites bearing postsynaptic sites turned into axons with presynaptic sites, with the axon initiation site on average located ~99 μm from the somata. Finally, all but one of the somata were located medial to stripe S1.

Neurons in this group had large dendritic arbors, with the dendrites arborizing over 22.5% of the total imaged volume (Figures S4A–S4C). The dendrites emerged laterally from somata and always extended ventrally. Only in one case were the dendrites observed to cross the midline, as indicated by the presence of postsynaptic sites confirming it as a dendrite (Figure 3A, Ipsi-only, arrowheads). The average diameter of dendrites was significantly larger as compared to the diameter of the axons (Figure 3F; $p < 2 \times 10^{-3}$, t test).

Contralateral Projection Only

Nine neurons distributed over the full RC extent, with the majority located at the caudal end of the imaged volume contained exclusively contralaterally projecting putative axons (Figure 3A, Contra-only). Like the axons in the ipsi-only group, the putative contralateral axons did not emerge as axons but started as a neurite with postsynaptic sites that became axonal. However, unlike the ipsi-only group, the axon initiation site was much closer to the somata. On average, the axon initiation site was located ~22 μm from the somata, which is significantly shorter than the axon initiation site for the ipsi-only group ($p < 0.0003$, t test). The somata of these neurons were located close to stripe S2.

The average dendritic length was ~290 μm (see also Table S1), and the dendritic arbors of these neurons arborized over 8% of the total volume (Figures S4A–S4C). This was significantly smaller than the dendritic arbors of the ipsi-only group ($p < 0.01$, t test). The average diameter of dendrites was significantly larger than the diameter of the axons (Figure 3F; $p < 2 \times 10^{-6}$, t test). The diameter of dendrites of the contra-only neurons was significantly smaller than the ipsi-only group (Figure 3F; $p < 0.005$, t test).

Projection Unknown

Seven neurons were located at the lateral-most extent of the animal. For these neurons, we did not find any neurites with

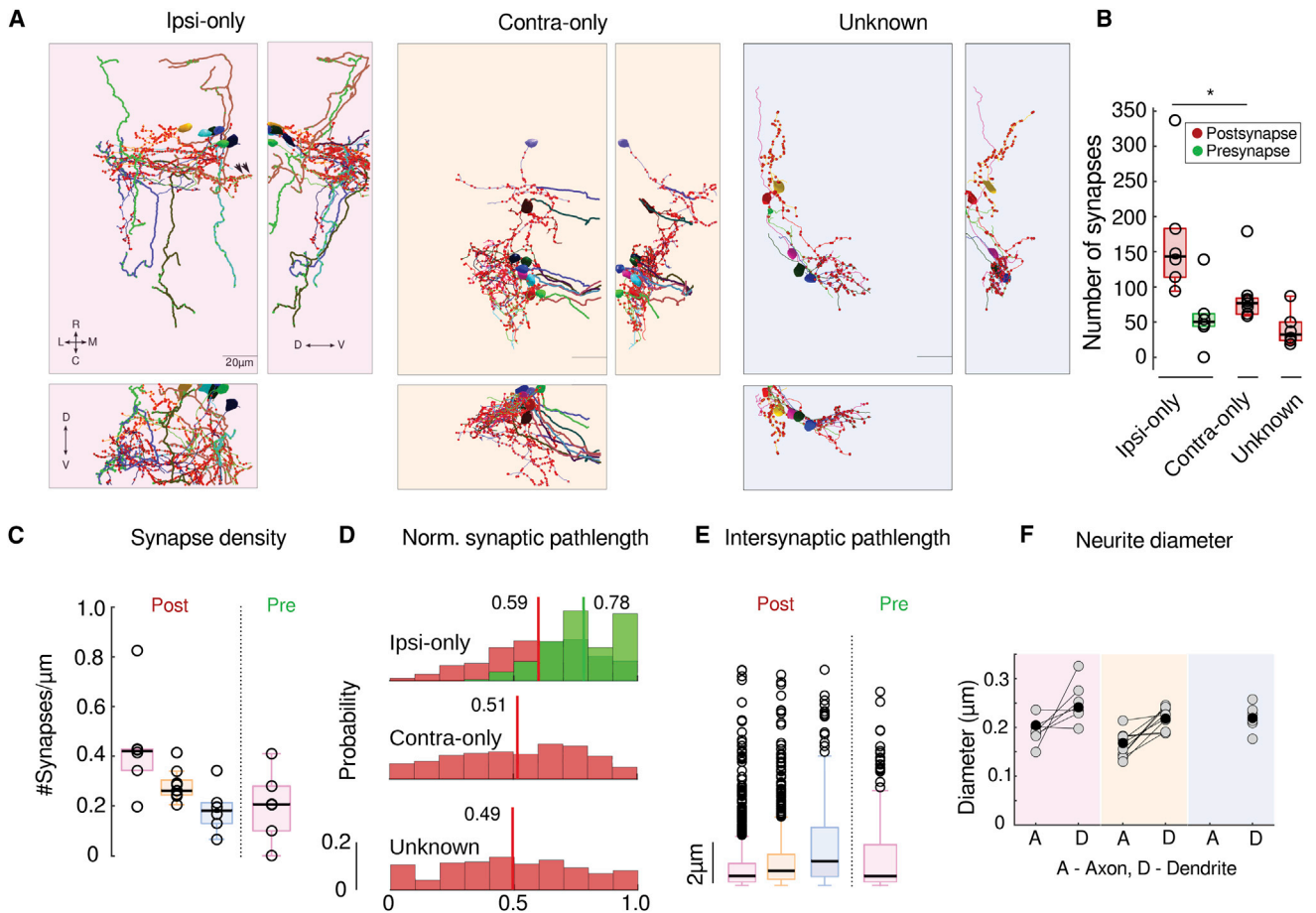


Figure 3. Integrator Neuron Projection Patterns and Synaptic Distribution

(A) Colored panels show three views of reconstructed integrator neurons, grouped according to their axonal projection patterns. Left: six integrator neurons with ipsilaterally projecting axons; ipsi-only group, pink background. Middle: nine integrator neurons with the midline crossing a contralaterally projecting putative axon; contra-only, orange background. Right: six integrator neurons with unknown axonal projection; unknown, blue background. Axons, dark lines; dendrites, light lines; postsynaptic sites, red circles; presynaptic sites, green circles.

(B) Boxplot of the number of synapses in each group (Ipsi-only, Contra-only, and Unknown). The black line is the median (* $p = 0.004$, Wilcoxon rank-sum test).

(C) Boxplot of the synaptic density for each group. Black lines indicate the medians.

(D) Normalized distribution of the synaptic path length. Postsynaptic sites, red; presynaptic sites, green. Colored vertical lines with adjoining numbers represent the means of the distribution.

(E) Boxplots of the intersynaptic path lengths for all four groups. Open circles are outliers, not shown beyond $10 \mu\text{m}$.

(F) Axonal and dendritic diameters of all neurons in each of the four groups. Gray dots are averages for each neuron, and black dots are averages per group. In (B), (C), and (E), the bottom and top edges of box plots represent the 25th and 75th percentile, respectively. The error bars represent the most extreme data points not considered as outliers.

See also [Figure S3](#).

presynaptic sites nor could we locate a putative axon (Figure 3A, Unknown). We believe this is most likely because these neurons were not fully represented in the imaged volume, and neurites of these neurons exited the volume before the axon was located. The average length of the dendrites for neurons from this group was $\sim 220 \mu\text{m}$ (see also [Table S1](#)), and they occupied on average $\sim 4.9\%$ of the total volume ([Figures S4A–S4C](#)).

Finally, one neuron had axons with both ipsilateral and contralateral projections ([Figure S4D](#)). This integrator neuron was located more lateral to the neurons from the ipsi-only group. The ipsilaterally projecting axon resembled the axons of the ipsi-only group of neurons ([Figure 3A](#)), with similar tilt in the RC axis. This neuron contained a neurite that crossed the midline.

We infer that this neurite is a putative contralaterally projecting axon based on the same cues that we used to identify other putative axons.

Organization of Integrator Neuron Synapses

Neurons from these three groups had on average 170, 84, and 40 postsynaptic (input) sites on their dendrites, respectively ([Figure 3B](#), red). The axons from the ipsi-only groups had approximately 58 presynaptic (output) sites ([Figure 3B](#), green). The path length of each synaptic location from the somata revealed that the distribution of the postsynaptic sites along the dendrites among the ipsi-only group was significantly different compared to the the contra-only and unknown groups, respectively

(Figure 3D; $p = 7.2 \times 10^{-13}$ and $p = 1.2 \times 10^{-10}$, Kolmogorov-Smirnov test).

We further computed the synaptic density, the number of synapses per unit length for all neurons, with the assumption that the synapses within each group were uniformly distributed along dendrites. The uniformity assumption was made because the distributions of the locations of postsynaptic sites were found to closely match the locations of dendritic arbors (Figure S4E). We found there were $\sim 1.5\times$ more input synapses on the ipsi-only group of neurons as compared to the inputs on the contra-only group of neurons (ipsi-only group, median number 0.42 inputs per μm ; contra-only group, 0.26 input per μm ; Figure 3C; $p = 0.049$, Wilcoxon rank-sum test). Empirically the average intersynaptic distances for the ipsi-only, contra-only, and unknown groups of neurons are 1 ± 2.3 , 1.2 ± 1.6 , and $2.6 \pm 4.5 \mu\text{m}$ with significantly different medians (Figure 3E; $p = 1.2 \times 10^{-10}$, $p = 1.1 \times 10^{-18}$, and $p = 5.2 \times 10^{-10}$, Wilcoxon rank-sum test).

Planar Organization of Synaptic Locations

The postsynaptic sites of the neurons from the ipsi-only and contra-only groups were observed to lie along orthogonal planes. The postsynaptic sites onto neurons from the ipsi-only group were noticed to lie roughly along a coronal plane with some tilt (Figure 3A). Similarly, the postsynaptic sites onto neurons from the contra-only neurons were noticed as exhibiting some planar organization as well. Fitting a plane through all of the postsynaptic sites revealed that these planes were nearly orthogonal (82.4°) to each other (Figure 4A).

The dendritic arbors and postsynaptic sites of neurons in these two groups displayed an inversion in their stratification depths. The dendritic arbors of the ipsi-only neurons on average were most abundant at $41.66 \pm 9.3 \mu\text{m}$ ventral to its somata (Figure 4B, top, pink line), whereas the contra-only group was maximal around $21.1 \pm 6.9 \mu\text{m}$ ventral to its somata (Figure 4B, bottom, orange line). The number of postsynaptic sites closely followed this inversion. Although relative to the bottom of the cranium, because many of the contra-only cells are more caudal and the brain is shallower, the depth profile may not be that different when viewed from a different origin.

Interestingly, when we overlaid the stripe patterns computed previously in Figure 1D with the stratification profiles of the synaptic sites along the ML axis, we found that the post- and pre-synaptic sites of the ipsi-only group were located medial to stripe S1 and lateral to S2, whereas the postsynaptic sites of the contra-only group were located very close to the intermediate stripe S2. Similar organization was observed for the other group of neurons (Figure S4F).

Connectivity between Integrator Neurons

We also examined the patterns of connectivity between integrator neurons. We found six synapses between integrator neurons: two synapses made by one ipsi-only neuron onto another ipsi-only neuron, and four synapses onto three contra-only neurons (Figure 4C). We found that there exist varying amounts of overlap of the axons of the ipsilaterally projecting neurons (Figure S4H) with the dendrites of all other neurons in the volume. Specifically, the overlap at ventro-rostral locations was from axons of ipsi-only neurons onto dendrites of other ipsi-only

neurons (Figure S4H, Ipsi→Ipsi), whereas the overlap at dorso-caudal locations was from axons of ipsi-only neurons onto dendrites of contra-only and the unknown group of neurons (Figure S4H, Ipsi→Contra, Ipsi→Unknown).

DISCUSSION

We combined two-photon calcium imaging of neurons in the larval zebrafish that were encoding for a behavioral variable (eye position) with serial-section EM. This was done by registering the LM volume to the EM volume to locate the same neurons. We were able to analyze in one animal 22 integrator neurons for which we had both functional and structural information. This procedure revealed the existence of distinct groups of neurons that make up the integrator circuit. This included an excitatory, ipsilaterally projecting group, an inhibitory, contralaterally projecting group, and a third, excitatory group, with unknown projections. Finally, we provide the first conclusive evidence for synapses between integrator neurons.

Of the 22 integrator neurons, 6 had exclusively ipsilaterally projecting axons. This population was most closely associated with the first somal stripe S1, which is thought to contain mostly excitatory, glutamatergic neurons [29]. The majority of synapses onto the dendrites of these neurons were along a plane approximately normal to the RC axis, whereas the axonal boutons of these neurons were oriented along the RC axis. This is reflected in the approximately orthogonal organization of the pre- and postsynaptic sites onto these neurons (Figure S4G). This suggests that these neurons are set up to sample broadly from axons that are oriented along the RC axis, including those from other integrator neurons. It has long been theorized that positive feedback via recurrent excitation could be a possible mechanism that can explain long persistent timescales of neuronal activity [26, 27, 43]. Indeed, we observed conclusive chemical synapses from one ipsilaterally projecting integrator neuron onto another ipsilaterally projecting integrator neuron. These facts point to the ipsi group of neurons as a candidate that could support positive feedback over recurrent excitation in the integrator circuit.

The second major group of neurons that we reconstructed was the nine contralaterally projecting neurons. The somatic locations of these neurons were most closely associated with the intermediate somal stripe S2, a grouping composed largely of GABAergic neurons at the DV depth investigated here [29]. The dendrites of these neurons arborized over a smaller area and stratified more dorsally as compared to the ipsilaterally projecting group of neurons. The postsynaptic inputs on the dendrites of these cells were along a plane that contained the RC axis. This suggests that these neurons sample narrowly from inputs along the RC axis. Inputs along the ML axis, however, would be sampled more broadly by these neurons. In the goldfish oculomotor integrator, contralaterally projecting neurons are thought to be involved in coordinating activity between the two sides, where each side acts as an independent integrator [9, 44]. Although we have not reconstructed the contralateral side of the axons, evidence from LM images of contralaterally projecting neurons shows projections that terminate in the dendritic field of the opposing population of inhibitory integrator neurons [29].

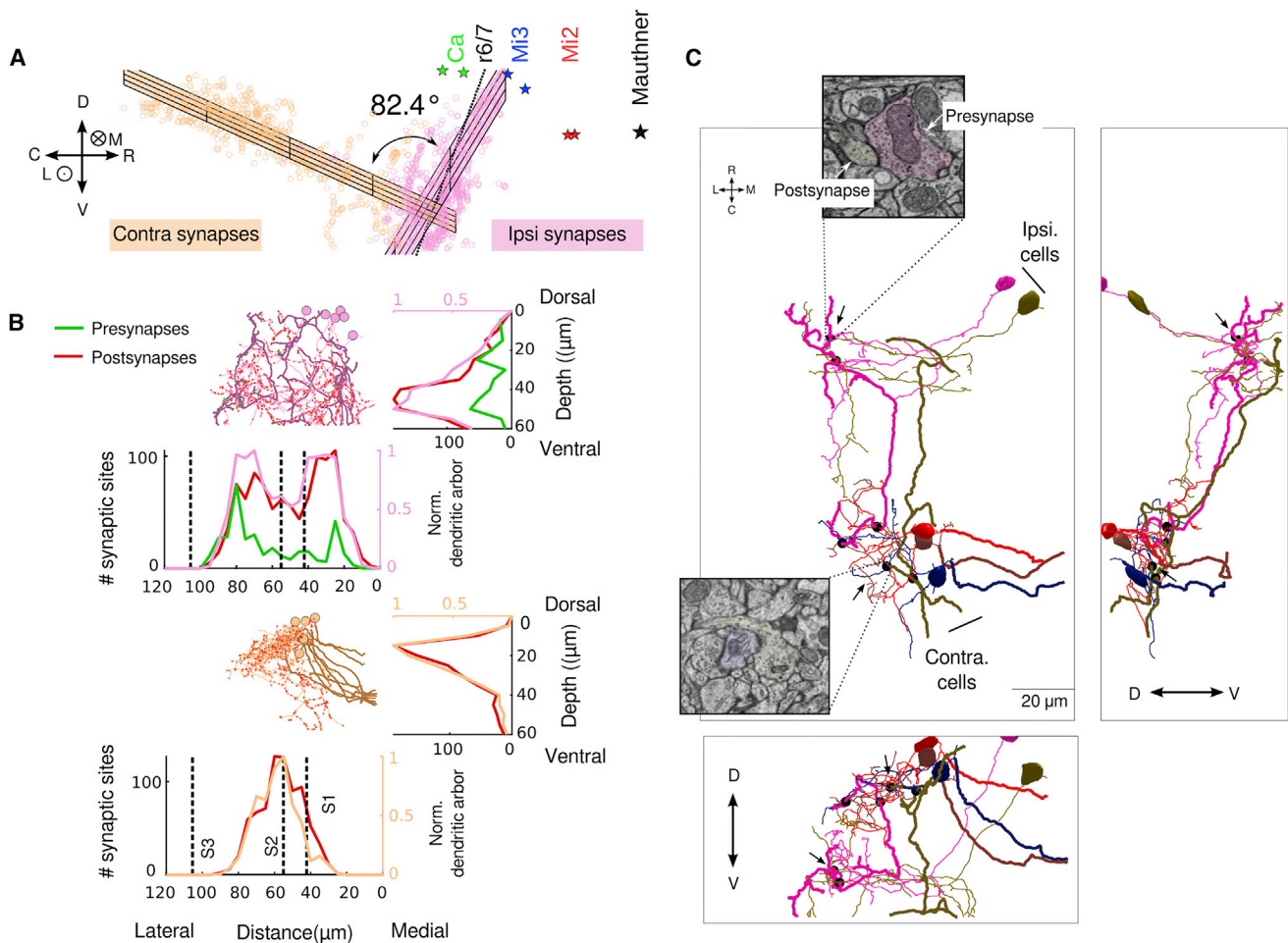


Figure 4. Integrator Neuron Organization and Connectivity

(A) Planar organization of ipsilaterally (pink) and contralaterally (orange) projecting neuron postsynaptic sites. The grid represents the best-fit plane through the cloud of points for each group. Anatomical landmarks: Mauthner neuron (black star), Mi2 (red stars), Mi3 (blue stars), and Ca (green stars). The black dotted line is the border between rhombomeres r6 and r7.

(B) Top: stratification profile of the all ipsi-only group of neurons. Two side views show the stratification of the dendrites and presynaptic and postsynaptic sites along the DV and ML axes. Dotted lines represent the location of the somatic peaks that was computed in Figure 1. Bottom: stratification profile of the all contra-only group of neurons.

(C) Three views of synaptically connected integrator neurons. Synapses from the ipsi-only group onto another neuron from the ipsi-only group (top left) (black circles) and from the ipsi-only group onto contra-only neurons (right). Black arrows indicate the location of the synapses, with insets showing the electron micrographs at two representative locations; colors in the insets are representative of the cells to which the synapses belong.

See also Figure S4.

The majority of the remaining integrator neurons were located at the lateral edge of the animal corresponding to the lateral-most stripe S3, where neurons are predominantly glutamatergic [32]. Because these neurons are close to the edge of the imaged volume, in all cases we were unable to trace many neurites from these cells; hence, the axonal projection pattern remains unknown. We also found one neuron, located along stripe S2, that had both an ipsilateral axon and a contralaterally projecting putative axon. The potential role of these neurons remains unknown.

The ipsilaterally projecting and the contralaterally projecting neurons differ in a number of properties. They have significantly different dendritic morphologies, axonal projections, and distributions of postsynaptic sites along their dendrites. The ipsi-

only group of neurons had approximately twice as many postsynaptic input sites as the contra-only group. In both cases, initiation of the axons was from a neurite that contained postsynaptic sites that then gave rise to presynaptic sites. This feature could be important to influence the activity of neurons, as these locations are proximal to the somata. For example, inhibitory synapses at such locations could have a shunting effect on the postsynaptic neuron. The integration time constants of these neurons show graded levels of persistent activity. Time constants of contralaterally projecting neurons were significantly different from the unknown projecting neurons, with the unknown projecting neurons showing faster dynamics (Figure S1D).

Our sample of 22 reconstructed integrator neurons is a fraction of the roughly 100 integrator neurons estimated to exist on

one side of the goldfish brain [45]. We observed six chemical synapses from two ipsilaterally projecting integrator neurons onto other integrator neurons. This observation may be an underestimate of integrator connectivity, for a few reasons. First, there are many neurons in the imaged volume that carried no usable fluorescence signal at all, largely because they did not take up enough calcium indicator. Some of these neurons are likely to be integrator neurons overlooked by our study, and are potential postsynaptic partners of the reconstructed neurons in our sample. Second, the imaged volume was limited in the DV extent. Thus, there were most likely integrator neurons outside the imaged volume, and they could receive synapses from our reconstructed integrator neurons. Furthermore, only three axonal arbors were fully or mostly reconstructed; the rest appeared substantially cut off as their axons left the volume. This is also evidenced by the fact that only two of the six ipsilaterally projecting axons project to the abducens motor nuclei, contrary to dye fill experiments, where all ipsilateral axons project to the abducens. Third, we had no possibility of finding connections between neurons on opposite sides of the brain, because only one side of the brain was imaged. Therefore, it is difficult to know whether the two neurons that made synapses onto other integrator neurons are an exceptional case or representative of a larger population that was incompletely sampled.

Here we present ultrastructural anatomical details of different types of integrator neurons and evidence of synaptic connectivity between these neurons, and present an approach that can be used to uncover general rules of connectivity and validate hypothesized theories of temporal integration. More definitive information about precise connectivity patterns between integrator neurons awaits a future experiment with an imaged volume that is large enough to encompass all integrator neurons and a fluorescent calcium indicator that labels a higher percentage of integrator neurons. Nonetheless, our findings to date can already be used to guide models of temporal integration with constraints in the form, density, and geometry of interactions between integrator neurons.

STAR★METHODS

Detailed methods are provided in the online version of this paper and include the following:

- [KEY RESOURCES TABLE](#)
- [CONTACT FOR REAGENT AND RESOURCE SHARING](#)
- [EXPERIMENTAL MODEL AND SUBJECT DETAILS](#)
- [METHOD DETAILS](#)
 - Two-photon calcium imaging
 - Serial section electron microscopy
 - Registration of light microscope and electron microscope volumes
 - Reconstructions
- [QUANTIFICATION AND STATISTICAL ANALYSIS](#)
- [DATA AND SOFTWARE AVAILABILITY](#)

SUPPLEMENTAL INFORMATION

Supplemental Information includes four figures and one table and can be found with this article online at <http://dx.doi.org/10.1016/j.cub.2017.06.028>.

AUTHOR CONTRIBUTIONS

Conceptualization, Methodology, & Writing, A.V., E.R.F.A., and H.S.S.; Formal Analysis, A.V. and H.S.S.; Data Curation, A.V.; Visualization, A.V.; Investigation, K.D. performed two-photon calcium imaging; A.V. acquired serial-section EM images with assistance from J.W.L. and assembled the resulting image stack; K.D. and A.D.R. registered the calcium images to the EM images; A.V. and E.R.F.A. reconstructed neurons with help from A.D.R.; Funding Acquisition, E.R.F.A. and H.S.S.

ACKNOWLEDGMENTS

We are grateful to Juan Carlos Tapia, Richard Schalek, and Ken Hayworth for assisting us with tissue preparation, the ATUM serial-sectioning procedure, and the WaferMapper software for EM imaging. Stephan Saalfeld, Albert Cardona, and Ignacio Arganda-Carreras answered questions about the TrakEM2 plugin for Fiji/ImageJ. Uygur Sümbül assisted with importing skeletons into MATLAB. We thank Jim Hudspeth for sharing reagents and tissue-processing protocols; Heather Sullivan for tissue processing and optimization; Ashleigh Showler, Gurion Marks, and Anjin Xianyu for assistance with reconstructions and alignment; and Melanie Lee for sharing light microscopic images of neurons. We benefited from helpful discussions with Jim Hudspeth, David Tank, and Kanaka Rajan. K.D. acknowledges the support of NIH training grant EY007138-16. E.R.F.A. acknowledges funding from the Burroughs Wellcome Career Award at the Scientific Interface, Searle Scholars Program, Simons Collaboration on the Global Brain, NSF CRCNS grant 1208088, and NIH grant R01027036. H.S.S. acknowledges funding from the Mathers Foundation, Gatsby Foundation, Human Frontier Science Program, NIH/NINDS award 5R01NS076467, and ARO MURI award W911NF-12-1-0594.

Received: December 21, 2016

Revised: March 2, 2017

Accepted: June 9, 2017

Published: July 13, 2017

REFERENCES

1. Briggman, K.L., Helmstaedter, M., and Denk, W. (2011). Wiring specificity in the direction-selectivity circuit of the retina. *Nature* **471**, 183–188.
2. Bock, D.D., Lee, W.C.A., Kerlin, A.M., Andermann, M.L., Hood, G., Wetzel, A.W., Yurgenson, S., Soucy, E.R., Kim, H.S., and Reid, R.C. (2011). Network anatomy and in vivo physiology of visual cortical neurons. *Nature* **471**, 177–182.
3. Lee, W.C., Bonin, V., Reed, M., Graham, B.J., Hood, G., Glattfelder, K., and Reid, R.C. (2016). Anatomy and function of an excitatory network in the visual cortex. *Nature* **532**, 370–374.
4. Major, G., and Tank, D. (2004). Persistent neural activity: prevalence and mechanisms. *Curr. Opin. Neurobiol.* **14**, 675–684.
5. Joshua, M., and Lisberger, S.G. (2015). A tale of two species: neural integration in zebrafish and monkeys. *Neuroscience* **296**, 80–91.
6. Friedrich, R.W., Jacobson, G.A., and Zhu, P. (2010). Circuit neuroscience in zebrafish. *Curr. Biol.* **20**, R371–R381.
7. Cannon, S.C., and Robinson, D.A. (1987). Loss of the neural integrator of the oculomotor system from brain stem lesions in monkey. *J. Neurophysiol.* **57**, 1383–1409.
8. Chéron, G., and Godaux, E. (1987). Disabling of the oculomotor neural integrator by kainic acid injections in the prepositus-vestibular complex of the cat. *J. Physiol.* **394**, 267–290.
9. Aksay, E., Olasagasti, I., Mensh, B.D., Baker, R., Goldman, M.S., and Tank, D.W. (2007). Functional dissection of circuitry in a neural integrator. *Nat. Neurosci.* **10**, 494–504.
10. Baker, R., Berthoz, A., and Delgado-García, J. (1977). Monosynaptic excitation of trochlear motoneurons following electrical stimulation of the prepositus hypoglossi nucleus. *Brain Res.* **121**, 157–161.

11. Baker, R., Delgado-Garcia, J., and Alley, K. (1977). Morphological and physiological demonstration that prepositus hypoglossi neurons terminate on medial rectus motoneurons. *Proc. Int. Union Physiol. Sci.* *11*, 49.
12. McCrea, R.A., Baker, R., and Delgado-Garcia, J. (1979). Afferent and efferent organization of the prepositus hypoglossi nucleus. *Prog. Brain Res.* *50*, 653–665.
13. Kaneko, C.R. (1999). Eye movement deficits following ibotenic acid lesions of the nucleus prepositus hypoglossi in monkeys II. Pursuit, vestibular, and optokinetic responses. *J. Neurophysiol.* *81*, 668–681.
14. McFarland, J.L., and Fuchs, A.F. (1992). Discharge patterns in nucleus prepositus hypoglossi and adjacent medial vestibular nucleus during horizontal eye movement in behaving macaques. *J. Neurophysiol.* *68*, 319–332.
15. Pastor, A.M., De la Cruz, R.R., and Baker, R. (1994). Eye position and eye velocity integrators reside in separate brainstem nuclei. *Proc. Natl. Acad. Sci. USA* *91*, 807–811.
16. Aksay, E., Baker, R., Seung, H.S., and Tank, D.W. (2000). Anatomy and discharge properties of pre-motor neurons in the goldfish medulla that have eye-position signals during fixations. *J. Neurophysiol.* *84*, 1035–1049.
17. Aksay, E., Gamkrelidze, G., Seung, H.S., Baker, R., and Tank, D.W. (2001). In vivo intracellular recording and perturbation of persistent activity in a neural integrator. *Nat. Neurosci.* *4*, 184–193.
18. van Alphen, A.M., Stahl, J.S., and De Zeeuw, C.I. (2001). The dynamic characteristics of the mouse horizontal vestibulo-ocular and optokinetic response. *Brain Res.* *890*, 296–305.
19. Robinson, D.A. (1989). Integrating with neurons. *Annu. Rev. Neurosci.* *12*, 33–45.
20. Robinson, D.A. (1970). Oculomotor unit behavior in the monkey. *J. Neurophysiol.* *33*, 393–403.
21. Leigh, R.J., and Zee, D.S. (2015). *The Neurology of Eye Movements* (Oxford University Press).
22. McCrea, R.A., and Baker, R. (1985). Cytology and intrinsic organization of the perihypoglossal nuclei in the cat. *J. Comp. Neurol.* *237*, 360–376.
23. Steiger, H.J., and Büttner-Ennever, J.A. (1979). Oculomotor nucleus afferents in the monkey demonstrated with horseradish peroxidase. *Brain Res.* *160*, 1–15.
24. Kamath, B.Y., and Keller, E.L. (1976). A neurological integrator for the oculomotor control system. *Math. Biosci.* *30*, 341–352.
25. Seung, H.S. (1996). How the brain keeps the eyes still. *Proc. Natl. Acad. Sci. USA* *93*, 13339–13344.
26. Seung, H.S., Lee, D.D., Reis, B.Y., and Tank, D.W. (2000). Stability of the memory of eye position in a recurrent network of conductance-based model neurons. *Neuron* *26*, 259–271.
27. Fisher, D., Olasagasti, I., Tank, D.W., Aksay, E.R.F., and Goldman, M.S. (2013). A modeling framework for deriving the structural and functional architecture of a short-term memory microcircuit. *Neuron* *79*, 987–1000.
28. Gonçalves, P.J., Arrenberg, A.B., Hablitzel, B., Baier, H., and Machens, C.K. (2014). Optogenetic perturbations reveal the dynamics of an oculomotor integrator. *Front. Neural Circuits* *8*, 10.
29. Lee, M.M., Arrenberg, A.B., and Aksay, E.R.F. (2015). A structural and genotypic scaffold underlying temporal integration. *J. Neurosci.* *35*, 7903–7920.
30. Miri, A., Daie, K., Burdine, R.D., Aksay, E., and Tank, D.W. (2011). Regression-based identification of behavior-encoding neurons during large-scale optical imaging of neural activity at cellular resolution. *J. Neurophysiol.* *105*, 964–980.
31. Higashijima, S., Mandel, G., and Fetcho, J.R. (2004). Distribution of prospective glutamatergic, glycinergic, and GABAergic neurons in embryonic and larval zebrafish. *J. Comp. Neurol.* *480*, 1–18.
32. Kinkhabwala, A., Riley, M., Koyama, M., Monen, J., Satou, C., Kimura, Y., Higashijima, S., and Fetcho, J. (2011). A structural and functional ground plan for neurons in the hindbrain of zebrafish. *Proc. Natl. Acad. Sci. USA* *108*, 1164–1169.
33. Koyama, M., Kinkhabwala, A., Satou, C., Higashijima, S., and Fetcho, J. (2011). Mapping a sensory-motor network onto a structural and functional ground plan in the hindbrain. *Proc. Natl. Acad. Sci. USA* *108*, 1170–1175.
34. Lee, R.K., Eaton, R.C., and Zottoli, S.J. (1993). Segmental arrangement of reticulospinal neurons in the goldfish hindbrain. *J. Comp. Neurol.* *329*, 539–556.
35. Kimura, Y., Okamura, Y., and Higashijima, S. (2006). *alx*, a zebrafish homolog of Chx10, marks ipsilateral descending excitatory interneurons that participate in the regulation of spinal locomotor circuits. *J. Neurosci.* *26*, 5684–5697.
36. Colombo, A., Reig, G., Mione, M., and Concha, M.L. (2006). Zebrafish BarH-like genes define discrete neural domains in the early embryo. *Gene Expr. Patterns* *6*, 347–352.
37. Jabeen, S., and Thirumalai, V. (2013). Distribution of the gap junction protein connexin 35 in the central nervous system of developing zebrafish larvae. *Front. Neural Circuits* *7*, 91.
38. Caley, D.W., and Butler, A.B. (1974). Formation of central and peripheral myelin sheaths in the rat: an electron microscopic study. *Am. J. Anat.* *140*, 339–347.
39. Rosenbluth, J., and Palay, S.L. (1961). The fine structure of nerve cell bodies and their myelin sheaths in the eighth nerve ganglion of the goldfish. *J. Biophys. Biochem. Cytol.* *9*, 853–877.
40. Barresi, M.J.F., Hutson, L.D., Chien, C.B., and Karlstrom, R.O. (2005). Hedgehog regulated Slit expression determines commissure and glial cell position in the zebrafish forebrain. *Development* *132*, 3643–3656.
41. Petralia, R.S., Wang, Y.X., Mattson, M.P., and Yao, P.J. (2015). Structure, distribution, and function of neuronal/synaptic spinules and related invaginating projections. *Neuromolecular Med.* *17*, 211–240.
42. Guemez-Gamboa, A., Coufal, N.G., and Gleeson, J.G. (2014). Primary cilia in the developing and mature brain. *Neuron* *82*, 511–521.
43. Joshua, M., Medina, J.F., and Lisberger, S.G. (2013). Diversity of neural responses in the brainstem during smooth pursuit eye movements constrains the circuit mechanisms of neural integration. *J. Neurosci.* *33*, 6633–6647.
44. Debowy, O., and Baker, R. (2011). Encoding of eye position in the goldfish horizontal oculomotor neural integrator. *J. Neurophysiol.* *105*, 896–909.
45. Aksay, E., Baker, R., Seung, H.S., and Tank, D.W. (2003). Correlated discharge among cell pairs within the oculomotor horizontal velocity-to-position integrator. *J. Neurosci.* *23*, 10852–10858.
46. Lister, J.A., Robertson, C.P., Lepage, T., Johnson, S.L., and Raible, D.W. (1999). *nacre* encodes a zebrafish microphthalmia-related protein that regulates neural-crest-derived pigment cell fate. *Development* *126*, 3757–3767.
47. Sümbül, U., Song, S., McCulloch, K., Becker, M., Lin, B., Sanes, J.R., Masland, R.H., and Seung, H.S. (2014). A genetic and computational approach to structurally classify neuronal types. *Nat. Commun.* *5*, 3512.
48. Cardona, A., Saalfeld, S., Schindelin, J., Arganda-Carreras, I., Preibisch, S., Longair, M., Tomancak, P., Hartenstein, V., and Douglas, R.J. (2012). TrakEM2 software for neural circuit reconstruction. *PLoS ONE* *7*, e38011.
49. Hayworth, K.J., Morgan, J.L., Schalek, R., Berger, D.R., Hildebrand, D.G.C., and Lichtman, J.W. (2014). Imaging ATUM ultrathin section libraries with WaferMapper: a multi-scale approach to EM reconstruction of neural circuits. *Front. Neural Circuits* *8*, 68.
50. Brustein, E., Marandi, N., Kovalchuk, Y., Drapeau, P., and Konnerth, A. (2003). “In vivo” monitoring of neuronal network activity in zebrafish by two-photon Ca(2+) imaging. *Pflugers Arch.* *446*, 766–773.
51. Smetters, D., Majewska, A., and Yuste, R. (1999). Detecting action potentials in neuronal populations with calcium imaging. *Methods* *18*, 215–221.

52. Miri, A., Daie, K., Arrenberg, A.B., Baier, H., Aksay, E., and Tank, D.W. (2011). Spatial gradients and multidimensional dynamics in a neural integrator circuit. *Nat. Neurosci.* *14*, 1150–1159.
53. Daie, K., Goldman, M.S., and Aksay, E.R.F. (2015). Spatial patterns of persistent neural activity vary with the behavioral context of short-term memory. *Neuron* *85*, 847–860.
54. Tapia, J.C., Kasthuri, N., Hayworth, K.J., Schalek, R., Lichtman, J.W., Smith, S.J., and Buchanan, J. (2012). High-contrast en bloc staining of neuronal tissue for field emission scanning electron microscopy. *Nat. Protoc.* *7*, 193–206.
55. Kasthuri, N., Hayworth, K.J., Berger, D.R., Schalek, R.L., Conchello, J.A., Knowles-Barley, S., Lee, D., Vázquez-Reina, A., Kaynig, V., Jones, T.R., et al. (2015). Saturated reconstruction of a volume of neocortex. *Cell* *162*, 648–661.
56. Longair, M.H., Baker, D.A., and Armstrong, J.D. (2011). Simple Neurite Tracer: open source software for reconstruction, visualization and analysis of neuronal processes. *Bioinformatics* *27*, 2453–2454.
57. Ma, L.H., Grove, C.L., and Baker, R. (2014). Development of oculomotor circuitry independent of hox3 genes. *Nat. Commun.* *5*, 4221.

STAR★METHODS

KEY RESOURCES TABLE

REAGENT or RESOURCE	SOURCE	IDENTIFIER
Experimental Models: Organisms/Strains		
Zebrafish: nacre(mitfa)	[46]	ZIRC (https://zfin.org/ZDB-ALT-010919-2)
Chemicals, Peptides, and Recombinant Proteins		
All EM reagents	EMSdiazum	N/A
Software and Algorithms		
Importing *.swc files	[47]	N/A
TrakEM2	[48]	N/A
Integrator firing rates	[30]	N/A
WaferMapper	[49]	N/A

CONTACT FOR REAGENT AND RESOURCE SHARING

For further information regarding the any resources and reagents please contact Ashwin Vishwanathan (ashwinv@princeton.edu).

EXPERIMENTAL MODEL AND SUBJECT DETAILS

All zebrafish larvae experimental procedures were approved by Weill Cornell Medical College's Institutional Animal Care and Use Committee. We used nacre mutant zebrafish larva, 6 days of age for all experiments.

METHOD DETAILS

Two-photon calcium imaging

A nacre mutant zebrafish larva, 6 days of age, was anesthetized in 100 mg/L tricaine-methanesulfonate (MS222, VWR TCT0941-025G) for about 1 min and then quickly mounted dorsal side up with droplets of 1.7% low temperature agarose (Sigma A0701-100G) on the lid of a 35mm petri dish containing a bed of hardened 1% agarose (Invitrogen 15510-027). The larva was then covered in 50 mg/L MS222. The larva was bulk-loaded [50, 51] with calcium sensitive dye Oregon Green 488 BAPTA-1 AM (5 mM, in DMSO with 5% pluronic, Invitrogen, O-6807) by inserting a capillary through the dorsal skin surface over the lateral edge of the right side of the hindbrain just caudal to the cerebellum, at $\sim 30^\circ$ decline relative to the dorsal surface. Following recovery, hindbrain of the animal was imaged at 790nm on predefined planes at 1 Hz. The imaging was performed unilaterally on three pre-defined planes $\sim 8 \mu\text{m}$ apart, below the level of the Mauthner neuron.

The integrator neurons were identified in a manner similar to a previously described method [52, 53]. Briefly, correlations for every pixel over a 5 min acquisition period was determined for eye position and eye velocity. A region-of-interest (ROI) was then drawn over the pixels where the majority were correlated to one of these variables. The fluorescence was reported as change in fluorescence for each frame relative to the average fluorescence, divided by the average. Saccadic fluorescence traces were displayed over an 8 s window starting 1 s before the end of the saccade. The firing rates were computed over a 6 s fixation period beginning 1 s after the end of the saccade. The firing rates were computed by deconvolving the average fluorescent traces with a calcium impulse response function (CIRF) as described previously [30]. The integrator time constants were calculated by fitting an exponential function (MATLAB ezfit) to the firing rates. The time constants for the fits were capped at 100 s.

Serial section electron microscopy

The animal was immersed in a fixative mixture of 2% paraformaldehyde and 2.25% glutaraldehyde buffered in 65 mM cacodylate buffer. The skin over the hindbrain was removed for good ultrastructure preservation and homogeneous staining of the tissue. Then it was thoroughly washed in 0.1M cacodylate buffer with 4% sucrose before staining. The tissue was stained using a conventional ROTO procedure [54]. Briefly, the specimen was stained in 1% reduced osmium tetroxide with potassium ferrocyanide for 2 hr on ice. The tissue was then washed 4x 30 min in 0.1M cacodylate buffer, also on ice. This was then followed by amplification in 1% sodium thiocarbonylhydrazide (TCH) for 15 min followed by 3x5 min washes in water and another round of incubation in 1% osmium tetroxide for 1 hr. The tissue was then washed 3x15 min in water and incubated with 1% aqueous uranyl acetate overnight. The following day the tissue was washed 3x15 min in water and incubated for 30 min in Lead aspartate solution, followed by washing and dehydration with a series of ethanol washes, followed by propylene oxide (PO) washes. The tissue was then infiltrated in decreasing gradients of PO and EPON for 24 hr and baked for 48 hr at 60 C. Following hardening, the tissue block face was coarsely

trimmed and a rectangular mesa was defined for serial sectioning. Care was taken to orient the specimen to permit sectioning along the horizontal axis. Serial sections from the above animal were collected approximately from the level of the Mauthner axon at a thickness of 45 nm. The serial sections were collected using the automatic tape-collecting ultramicrotome (ATUM) [49, 55]. The serial sections were then adhered to a silicon wafer, using double sided carbon tape (TEDpella), the wafers were coated with a thin film of carbon to make them conductive. Each wafer was imaged in a Zeiss Sigma field emitting scanning electron microscope in the backscattered electron mode using a custom software interface to collect the images [49]. For the high-resolution each section was imaged at a lateral resolution of 5nm/pixel in a region of interest that roughly corresponded with the area imaged on the light microscopic. The EM volume we imaged contained 15791 image tiles (8000 × 8000 pixels each) or $\sim 10^{11}$ pixels. The imaged volume was $220 \times 112 \times 57 \mu\text{m}^3$ (RC X ML X DV).

Registration of light microscope and electron microscope volumes

The EM images were aligned using the TrakEM2 plugin in Fiji [48]. Briefly, individual images were imported into the TrakEM2 framework and montaged using affine and elastic transforms. The images were then registered in z using a similar approach, where the first pass was performed using affine transforms, followed by elastic transforms. All the alignment was performed on a machine with 32 virtual cores and 120GB RAM.

To locate the cells that were involved in the integrator circuit, we first made use of the fact that gross morphological features including blood vessels and the mauthner axon were easily identified in both the LM and EM stacks. Once enough such features were identified in the LM stack, interpolated at EM step sizes, we located these same landmarks in the high-res EM stack. Each pair of landmarks (one from the LM volume and one from the EM volume) was then used to calculate a global affine transform that was applied to transform the LM volume to be overlaid on the EM volume using the TrakEM2 plugin in Fiji [48]. Following this first round of registration, we then identified 7 cells at different locations throughout the volume that were easily identified in both datasets and performed a second round of alignment.

Reconstructions

The reconstruction of the identified neurons was performed using the TrakEM2 plugin in Fiji/ImageJ. One expert (AV) traced all neurons and annotated all pre- and postsynaptic sites. A second expert (EA) identified locations at which the skeletons looked unusual (sharp turns or closely spaced branch points). EA reviewed the images at all of these locations (typically a few per neuron), and reached consensus with AV. A few locations were judged ambiguous in the sense that image defects made it impossible to interpret the locations with certainty. At such ambiguous locations, we erred on the side of incomplete tracing.

A second round of tracing was then carried out using a semi-automated, volume based reconstruction method similar to the ‘eyewire’ platform (<http://eyewire.org>). This process involved semiautomatic reconstruction of neurons with two tracers (not the authors), where the second tracer was able to view the first tracer’s reconstructions. A third expert tracer (A.V) reviewed all sites where the first two tracers differed to provide consensus. The final trace included all those neurites where the majority agreed. This ensured that each cell was covered by at least 2 tracers. This semi-automated process revealed that the axon of one cell was previously under-reconstructed and another dendrite from a different cell was over-reconstructed. The remaining 20/22 cells remained the same between both methods.

Having real-time volume based tracing provides shape based context to tracers. This is useful to detect error. For example, if a neurite is falsely merged it is often the case that its diameter is different as compared to the neurite being reconstructed. Similarly, at locations where the neurites are very thin, we can often reconstruct all the neurites abutting the neurite being traced to eliminate false positives,

Since the section thickness was 45nm, neurites that were parallel to the cutting plane were sometimes hard to follow during reconstruction. This typically leads to problems when tracing very thin neurites (typically axons) that can be hard to follow. In such instances it is useful to keep track of internal organelles and other cues such as contrast to eliminate ambiguous locations. After such techniques are applied, the end result is that every cell has at most one or two truly ambiguous locations. The ambiguity might be caused by a thin neurite parallel to the sectioning plane, or deteriorated ultrastructure (due to electroporation, poor fixation, or possibly developmental pruning of axons). In truly ambiguous locations, we err on the side of undertracing.

The skeletonized tree structure was exported from TrakEM2 as *.swc files. These trees were then imported into MATLAB using custom scripts to import .swc files as trees. For the comparison of EM traces with LM traces, the LM traces were traced using the Simple Neurite Tracer [56] plugin in Fiji, and exported as *.swc file. In total, we reconstructed 9.29 mm of neurite (2.45 mm of axonal length and 6.84 mm of dendritic length).

QUANTIFICATION AND STATISTICAL ANALYSIS

All tree lengths are reported as pathlengths unless noted otherwise. Similarly, all lengths to a pre- or postsynaptic site are reported as pathlengths. We defined the axon initiation site as the parent node of the first presynaptic site. All neurites that are not axonal are defined as dendritic. All nodes of the tree were thus divided as axonal nodes or dendritic nodes. Pathlengths were generated for a tree over all axonal nodes or all dendritic nodes, and the length of the tree was the sum of all axonal length and dendritic length. A collateral

was defined as all those segments of an axon, that emerged from the central axonal shaft. All axonal nodes were divided into collateral and non-collateral nodes. The completeness of cells was decided based on the number of neurites that exited the cells, the fewer that exited, the more complete the cell,

The diameter of the axon and dendrites for each tree was generated by drawing a line segment along the cross-section at random locations along the tree. Many such line segments were drawn across the entire extent of the tree. The values are reported as a mean across all dendrites and axons.

Arbor densities of the dendrites was computed by projecting all the axonal or dendritic nodes along the desired plane and reported in a normalized scale. Arbor volumes were computed using the MATLAB function `convhull`. To infer the neurotransmitter identity from the stripe organization of the cell bodies, we annotated the location of all the cell bodies from a low-resolution stack. The cell density was then computed by projecting all the cells along the desired axis. This process picked out the peaks that were visible in the EM images. The location of a stripe was defined as the local peak that emerged from the cell density projecting analysis. The planar organization of the postsynapses and presynapses were fit to a plane using the `planefit` function, available on the MATLAB central repository.

To locate the border between r6 and r7 we followed a similar approach that was performed previous using light microscopic imaging and the expression of the hox genes [29, 53, 57]. Briefly reticulospinal cells were identified based on the ultrastructure, that was very different from the remaining cells in the area. These cells were rich in mitochondria and gave rise to a large myelinated axon that joined the medial longitudinal fasciculus. We fit a plane to the reticulospinal neurons, and identified a point on this plane that bisected Mi3 neuron located in r6 and Ca neuron located in r7. The tilt of this border from previous studies was observed to be 0.37 based on transgene expression patterns. This line that bisected the locations of Mi3 and Ca was moved 0.37 μm caudally for every micron ventrally based on [29, 53]. The resulting line is where we differentiate the border of r6 and r7.

DATA AND SOFTWARE AVAILABILITY

All reconstructed neuron traces will be uploaded to the <http://neuromorpho.org> repository for download. The traces can be imported and analyzed using the MATLAB tool box for analysis, <http://treestoolbox.org>.